Dynamic Behavior and Force Analysis of the Full Vehicle Model using Newmark Average Acceleration Method

Engin Yildirim
Faculty of Engineering
Department of Mechanical Engineering
Karabuk University
Karabuk, Turkey
enginyildirim@karabuk.edu.tr

Ismail Esen
Faculty of Engineering
Department of Mechanical Engineering
Karabuk University
Karabuk, Turkey
iesen@karabuk.edu.tr

***Abstract*—In this study, the dynamic interaction between road and vehicle is modeled. For this purpose, a full vehicle model with eight degrees of freedom is considered. The equations of motion of the whole system are derived by the D'Alambert method and numerical solutions are obtained by the Newmark average acceleration method. Due to varying road roughness, the forces affecting the driver and the vehicle-components are analyzed in detail. Also, vertical and rotational displacements, velocities, and accelerations are examined, and results graphs are given. Two different pre-defined road profiles, created as non-random road excitation, and five different vehicle speeds are presented and analyzed.**

Keywords-vehicle road interaction; full-vehicle model; passenger comfort; dynamic forces on vehicle components

I. INTRODUCTION

Vehicle dynamics and forces affecting vehicle components and driving comfort with increasing vehicle speed are an emerging research topic. Many vehicle models have been proposed to examine vehicle-road interaction. Generally, these models can be classified in three types, quarter-car, half-car, and full-car modeling. Using Taguchi L16 array and SNR analysis, measurements for the performance of the semi-active suspension system with MR damper were taken in [1] and according to the results, damper cylinder material is the key parameter to the design of the magnetorheological (MR) damper. By using speed bump as road disturbance, overshoot and settling time with passive suspension system were analyzed in [2] for a quarter-car model with 2 degrees of freedom. Adding an inerter on the suspension system, the performance of vibration absorbing was investigated in [3]and the vibration was considerably decreased. A robust quarter-car control scheme was created in [4] along with a road disturbance profile with a sliding mode controller. According to the variable damping coefficient limit, semi-active suspension systems were created in Matlab/Simulink in [5] and system's damping coefficient limit of 4000Ns/m performed best when considering ride comfort. Theoretical and experimental analyses of rail vehicles were modeled in [6] using electro-mechanic similarity theory. A quarter-car model with a PID controller used to minimize the vertical body acceleration was prepared in [7]. A method was developed in [8] for the performance optimization of an eCAR considering the impact of road dynamics, acceleration rate, mass changing and gear ratio. According to the results, the proposed method was efficient and simple and could be applied to any eCAR model. An active suspension system which used sliding mode control was created and compared with the passive suspension system in [9]. The results show that this system has better effect on vibration isolation compared to the passive suspension system.

A Grey Fuzzy Sliding Mode controller was proposed in [10] for improving ride comfort. The results show that this controller provides robustness to the system under the presence of uncertainties. Under three different road roughness classes classified by the ISO-8608 standard, Newmark Beta method was used in [11] for quarter-car analysis. Under step road roughness, the suspension system of a quarter-car model was analyzed in [12]. The results show that ride comfort was not suitable according to the ISO2631-1 standard. For half-car suspension system analysis, ADAMS/Car program was used and B class road and pulse input were utilized as road disturbance in [13]. A nonlinear half-car model was created in [14] and for reducing the vibration levels PID control, Fuzzy Logic Control (FLC), Hybrid Fuzzy-PID control (HFPID), and Hybrid Fuzzy Logic controller with Coupled Rules (HFPIDCR) have been used. According to the simulation results the HFPIDCR shows good performance in reducing the vibration levels under nonlinear system parameters. A half-car model with road adaptive nonlinear control was created in [15] with road adaptive algorithm schemes, showing adaptation potential for different road types. Active and passive suspension systems of a half-car model were analyzed in [16] using nonlinear suspension stiffness and damping. The results showed that the nonlinear active suspension system performed better when compared with the passive one. A full-car model with seven degrees of freedom with nonlinear suspension springs and dampers under sinusoidal road disturbances was studied in [17] and according to the results the car response

Corresponding author: Engin Yildirim

could be chaotic. The suspension system of a full-car model was examined in [18] using three different road assumptions, while a full-car model was analyzed in [19] for passive and active suspension systems under a sinusoidal road excitation with optimization technique.

Using a bump road excitation as a road roughness model, a semi active control algorithm was used in [20] for a full-car model with an MR damper. The results show that this control algorithm decreases displacements and accelerations. For optimization of ride comfort and handling, a semi-active control was created in [21] using a full-car model. According to the results, this algorithm achieved the intended goals. A quasi-LPV approach was studied in [22] as a semi-active controller for seven degrees of freedom of a full-car model. For a semi-active full-car model, LQ controller and observer were compared in [23] with a real vehicle with a skyhook controller. An H∞ observer was designed in [24] to decrease the effects of unknown ground disturbances on the full-car model with seven degrees of freedom. Ride comfort and frequency response up to 18Hz of a full-car model with ten degrees of freedom were examined in [25]. For road profile irregularities estimation a new technique called Independent Component Analysis (ICA) was proposed in [26]. The obtained results show that the proposed technique is adequate for identifying road disturbances. Optimization of the passive suspension system was examined in [27], and for this purpose, a numerical-computational program was developed. Driver seat vertical acceleration was reduced approximately by 21.14% of weighted RMS value. A robust finite-frequency H∞ controller was developed and studied in [28]. The fundamentals of full-car dynamics and the vibration influence to the human body in order to design better active suspension systems for suitable comfort level were investigated in [29]. A full-car model with seven degrees of freedom and an MR dumper was analyzed in [30] for suspension system control. The control algorithm included optimal control algorithm and Fuzzy Logic, Linear Quadratic Regulator (LQR) and Fuzzy controller.

In this study an accurate modeling of vehicle road interaction using a full-car model which can be used for the investigation of vertical, pitch, and roll movements of the car body, driver's seat and other suspension components, is presented. In addition, as an issue which has not been discussed in detail in the literature, the analysis of the forces applied to both the vehicle body and the driver's seat was also conducted. Newmark average acceleration method was used as a different method than the ones generally used for these studies. In addition, in order to examine the effects of vehicle speed on vehicle dynamics, analysis was performed at 5 different vehicle speeds. For this purpose, analysis was performed for two different proposed road roughness models.

II. MATHEMATICAL MODELING

To study vehicle dynamics and dynamic forces affecting vehicle components, the vehicle could be classified in one of the three different models which are (from the least to the most complex): quarter-car, half-car, and full-car. In this study the full-car model was used because it is the nearest to real-life vehicles (Figure 1). In this model, roll and pitch rotation movements can be examined along with vertical movements and forces.

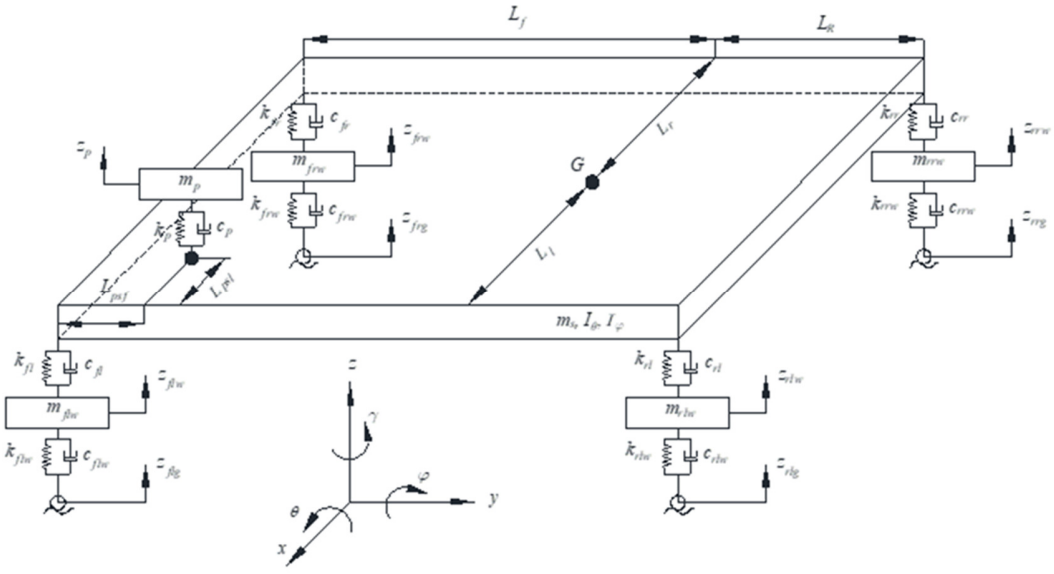

Fig. 1. The full vehicle model

The full-car model has eight degrees of freedom and includes passenger mass m_p, car body mass m_s, front left wheel mass m_{flw}, rear left wheel mass m_{rlw}, front right wheel mass m_{frw}, rear right wheel mass m_{rrw}, moment of inertia of pitch I_θ, moment of inertia of roll I_φ, and connecting elements which comprise of dampers and springs with the same properties and linear characteristics. In this system, springs are named as: passenger seat stiffness k_p, front left suspension stiffness k_{fl}, rear left suspension stiffness k_{rl}, front right suspension stiffness k_{fr}, rear right suspension stiffness k_{rr}, front left wheel stiffness

k_{flw}, rear left wheel stiffness k_{rlw}, front right wheel stiffness k_{frw}, and rear right wheel stiffness k_{rrw}, all with linear characteristics. Similarly, dampers were named as: passenger seat damping coefficient c_p, front left suspension damping coefficient c_{fl}, rear left suspension damping coefficient c_{rl}, front right suspension damping coefficient c_{fr}, rear right suspension damping coefficient c_{rr}, front left wheel damping coefficient c_{flw}, rear left wheel damping coefficient c_{rlw}, front right wheel damping coefficient c_{frw}, rear right damping coefficient c_{rrw}, all with linear characteristics. G is the center of gravity of the full-car body. This system has both vertical and rotational displacements, and so it needs reference directions for these displacements. Vertical displacements were symbolized as: passenger vertical displacement z_p, center of car body vertical displacement z_f, front left wheel vertical displacement z_{flw}, rear left wheel vertical displacement z_{rlw}, front right wheel vertical displacement z_{frw}, rear right wheel vertical displacement z_{rrw}, pitch rotational movement θ, and roll rotational movement φ. Also, road roughness effects on vertical displacement were symbolized as z_{flg}, z_{rlg}, z_{frg}, z_{rrg}, representing front left road, rear left road, front right road, and rear right road respectively. Basic measurements of passenger and center of gravity of the car body are shown in Figure 1. G is the location of the center of gravity, L_f, L_R, L_l, and L_r are the distances of G from the front of the car body, rear of the car body, left of the car body and right of the car body respectively. Passenger distances from the left and the front of the car body are symbolized as L_{psf} and L_{psl} respectively. Rotation movements occur around each direction on Cartesian coordinates. Pitch (θ), roll (φ), and yaw (γ) movements occur around x, y, and z axes respectively. Because cornering situation was not considered, the yaw movement was not studied in this analysis. The motion equations are given below:

$$m_p\ddot{z}_p + c_p\left[\dot{z}_p - \dot{z}_f + \left(L_f - L_{psf}\right)\dot{\theta} + \left(L_{psl} - L_l\right)\dot{\varphi}\right] + k_p\left[z_p - z_f + \left(L_f - L_{psf}\right)\theta + \left(L_{psl} - L_l\right)\varphi\right] = 0 \quad (1)$$

$$\begin{aligned} m_s\ddot{z}_f - c_p\left[\dot{z}_p - \dot{z}_f + \left(L_f - L_{psf}\right)\dot{\theta} + \left(L_{psl} - L_l\right)\dot{\varphi}\right] - k_p\left[z_p - z_f + \left(L_f - L_{psf}\right)\theta + \left(L_{psl} - L_l\right)\varphi\right] + c_{fl}\left(\dot{z}_f - L_f\dot{\theta} + L_l\dot{\varphi} - \dot{z}_{flw}\right) \\ + k_{fl}\left(z_f - L_f\theta + L_l\varphi - z_{flw}\right) + c_{rl}\left(\dot{z}_f + L_R\dot{\theta} + L_l\dot{\varphi} - \dot{z}_{rlw}\right) + k_{rl}\left(z_f + L_R\theta + L_l\varphi - z_{rlw}\right) \\ + c_{fr}\left(\dot{z}_f - L_f\dot{\theta} - L_r\dot{\varphi} - \dot{z}_{frw}\right) + k_{fr}\left(z_f - L_f\theta - L_r\varphi - z_{frw}\right) + c_{rr}\left(\dot{z}_f + L_R\dot{\theta} - L_r\dot{\varphi} - \dot{z}_{rrw}\right) \\ + k_{rr}\left(z_f + L_R\theta - L_r\varphi - z_{rrw}\right) = 0 \end{aligned} \quad (2)$$

$$\begin{aligned} I_\theta\ddot{\theta} - \dot{z}_p\left[c_p\left(L_{psf} - L_f\right)\right] - \dot{z}_f\left[\left(c_{fl} + c_{fr}\right)L_f - \left(c_{rl} + c_{rr}\right)L_R + c_p\left(L_f - L_{psf}\right)\right] - \dot{\theta}\left[-\left(c_{fl} + c_{fr}\right)L_f^2 - \left(c_{rl} + c_{rr}\right)L_R^2 - c_p\left(L_f - L_{psf}\right)^2\right] \\ - \dot{\varphi}\left[\left(c_{fl}L_l - c_{fr}L_r\right)L_f + \left(c_{rr}L_r - c_{rl}L_l\right)L_R + c_p\left(L_l - L_{psl}\right)\left(L_f - L_{psf}\right)\right] + \dot{z}_{flw}c_{fl}L_f + \dot{z}_{frw}c_{fr}L_f - \dot{z}_{rlw}c_{rl}L_R \\ - \dot{z}_{rrw}c_{rr}L_R - z_p\left[k_p\left(L_{psf} - L_f\right)\right] - z_f\left[\left(k_{fl} + k_{fr}\right)L_f - \left(k_{rl} + k_{rr}\right)L_R + k_p\left(L_f - L_{psf}\right)\right] \\ - \theta\left[-\left(k_{fl} + k_{fr}\right)L_f^2 - \left(k_{rl} + k_{rr}\right)L_R^2 - k_p\left(L_f - L_{psf}\right)^2\right] \\ - \varphi\left[\left(k_{fl}L_l - k_{fr}L_r\right)L_f + \left(k_{rr}L_r - k_{rl}L_l\right)L_R + k_p\left(L_l - L_{psf}\right)\left(L_f - L_{psf}\right)\right] + z_{flw}k_{fl}L_f + z_{frw}k_{fr}L_f - z_{rlw}k_{rl}L_R \\ - z_{rrrw}k_{rr}L_R = 0 \end{aligned} \quad (3)$$

$$\begin{aligned} I_\varphi\ddot{\varphi} - \dot{z}_p\left[c_p\left(L_l - L_{psl}\right)\right] - \dot{z}_f\left[\left(c_{fr} + c_{rr}\right)L_r - \left(c_{fl} + c_{rl}\right)L_l + c_p\left(L_{psl} - L_l\right)\right] \\ - \dot{\theta}\left[\left(c_{rr}L_R - c_{fr}L_f\right)L_r + \left(c_{fl}L_f - c_{rl}L_R\right)L_l + c_p\left(L_f - L_{psf}\right)\left(L_l - L_{psl}\right)\right] \\ - \dot{\varphi}\left[-\left(c_{fr} + c_{rr}\right)L_r^2 - \left(c_{fl} + c_{rl}\right)L_l^2 - c_p\left(L_{psl} - L_l\right)^2\right] + \dot{z}_{frw}c_{fr}L_r + \dot{z}_{rrw}c_{rr}L_r - \dot{z}_{flw}c_{fl}L_l - \dot{z}_{rlw}c_{rl}L_l \\ - z_p\left[k_p\left(L_l - L_{psl}\right)\right] - z_f\left[\left(k_{fr} + k_{rr}\right)L_r - \left(k_{fl} + k_{rl}\right)L_l + k_p\left(L_{psl} - L_l\right)\right] \\ - \theta\left[\left(k_{rr}L_R - k_{fr}L_f\right)L_r + \left(k_{fl}L_f - k_{rl}L_R\right)L_l + k_p\left(L_f - L_{psf}\right)\left(L_l - L_{psl}\right)\right] \\ - \varphi\left[-\left(k_{fr} + k_{rr}\right)L_r^2 - \left(k_{fl} + k_{rl}\right)L_l^2 - k_p\left(L_{psl} - L_l\right)^2\right] + z_{frw}k_{fr}L_r + z_{rrw}k_{rr}L_r - z_{flw}k_{fl}L_l - z_{rlw}k_{rl}L_l = 0 \end{aligned} \quad (4)$$

$$m_{flw}\ddot{z}_{flw} - c_{fl}\left(\dot{z}_f - L_f\dot{\theta} + L_l\dot{\varphi} - \dot{z}_{flw}\right) - k_{fl}\left(z_f - L_f\theta - L_l\varphi - z_{flw}\right) + c_{flw}\left(\dot{z}_{flw} - \dot{z}_{flg}\right) + k_{flw}\left(z_{flw} - z_{flg}\right) = 0 \quad (5)$$

$$m_{rlw}\ddot{z}_{rlw} - c_{rl}\left(\dot{z}_f + L_R\dot{\theta} + L_l\dot{\varphi} - \dot{z}_{rlw}\right) - k_{rl}\left(z_f + L_R\theta + L_l\varphi - z_{rlw}\right) + c_{rlw}\left(\dot{z}_{rlw} - \dot{z}_{rlg}\right) + k_{rlw}\left(z_{rlw} - z_{rlg}\right) = 0 \quad (6)$$

$$m_{frw}\ddot{z}_{frw} - c_{fr}\left(\dot{z}_f - L_f\dot{\theta} - L_r\dot{\varphi} - \dot{z}_{frw}\right) - k_{fr}\left(z_f - L_f\theta - L_r\varphi - z_{frw}\right) + c_{frw}\left(\dot{z}_{frw} - \dot{z}_{frg}\right) + k_{frw}\left(z_{frw} - z_{frg}\right) = 0 \quad (7)$$

$$m_{rrw}\ddot{z}_{rrw} - c_{rr}\left(\dot{z}_f + L_R\dot{\theta} - L_r\dot{\varphi} - \dot{z}_{rrw}\right) - k_{rr}\left(z_f + L_R\theta - L_r\varphi - z_{rrw}\right) + c_{rrw}\left(\dot{z}_{rrw} - \dot{z}_{rrg}\right) + k_{rrw}\left(z_{rrw} - z_{rrg}\right) = 0 \quad (8)$$

III. MODELING OF ROAD ROUGHNESS

The analysis of the effect of the bump height on the vehicle dynamics and of the force on vehicle components for two different road profiles is shown in Figures 2-3. In the model illustrated in Figure 2, the amplitude of the first bump is higher than the amplitude of the second bump. The mathematical expression is given in (9), where *E1*, *E2* represent the amplitudes and *G1*, *G2* represent the widths of the road defects. In (9), *T1=B+G1* and *T2=B+G1+A+G2*. In the second model (Figure 3), the amplitudes of the irregularities in the road are the same. The mathematical expression is given in (12) [31].

$$r(x) = \begin{cases} \frac{1}{2}E1\left(1 - \cos\left(\frac{2\pi(x - B - G1)}{G1}\right)\right), & for\ B \le x \le B + G1 \\ \frac{1}{2}E2\left(1 - \cos\left(\frac{2\pi(x - B - G1 - A)}{G2}\right)\right), & for\ T1 + A \le x \le T2 \\ 0, & elsewhere \end{cases} \quad (9)$$

$$r(x) = \begin{cases} \frac{1}{2}E\left(1 - \cos\left(\frac{2\pi(x - C)}{D}\right)\right), & for\ C \le x \le C + D \\ 0 & elsewhere \end{cases} \quad (10)$$

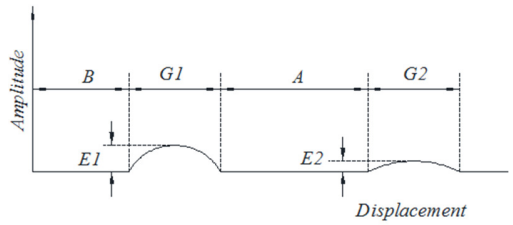

Fig. 2. The first road irregularity model

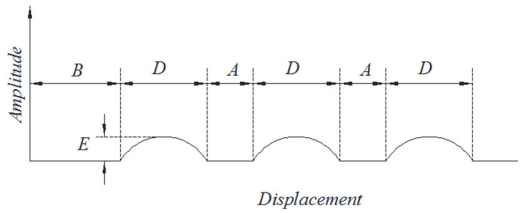

Fig. 3. The second road irregularity model

IV. NUMERICAL ANALYSIS

For the numerical analysis of the full vehicle model, a Matlab program that includes vehicle and road parameters and Newmark average acceleration method [32] was created. The used full-car model parameters are given in Table I. The road profiles' parameters are given in Table II.

TABLE I. PARAMETERS OF THE FULL VEHICLE MODEL

Parameter	Value	Unit
Passenger and seat mass	80	kg
Car body mass	1500	kg
Wheel mass	50	kg
Car body's moment of inertia on x axis	1680	kgm^2
Car body's moment of Inertia on y axis	1500	kgm^2
Seat damping coefficient	600	Ns/m
Front damping coefficient	1200	Ns/m
Rear damping coefficient	1000	Ns/m
Front wheel damping coefficient	60	Ns/m
Rear left wheel damping coefficient	50	Ns/m
Seat suspension stiffness	8000	N/m
Front suspension stiffness	30000	N/m
Rear suspension stiffness	20000	N/m
Front wheel suspension stiffness	150000	N/m
Rear wheel suspension stiffness	120000	N/m
Center of gravity - left wheel distance	0.75	m
Center of gravity - right wheel distance	0.75	m
Center of gravity - front wheel distance	1.4	m
Center of gravity - rear wheel distance	1.1	m
Passenger - left wheel distance	0.4	m
Passenger - front wheel distance	1	m

TABLE II. ROAD PARAMETERS

First road irregularity profile		Second road irregularity profile	
Parameters	**Values**	**Parameters**	**Values**
B	5m	B	10m
A	10m	A	3m
G1	1m	D	0.3m
G2	1m	E	0.05m
E1	0.1m		
E2	0.05m		

V. RESULTS

The effects of speed bumps, on the dynamics of the vehicle were examined for five different vehicle speeds and two road profiles. These speeds were taken as 60km/h, 90km/h, 120km/h, 150km/h, and 180km/h respectively.

A. Results of the First Road Irregularity

The first road irregularity profile is given in Figure 2. Under this road irregularity, passenger seat vertical displacement and car body vertical, pitch, and roll displacements are shown in Figure 4, for five different vehicle velocities. When vehicle speed increased, all displacement values decreased, and peak point locations occurred more at the right side, for all displacement figures because of the increase in the taken road during the period of oscillation. Passenger seat displacement values are higher than car body's and this situation shows that passenger seat stiffness and damping coefficients could have more suitable values. But compared with road irregularities, more than 80% of disturbances of the road are isolated according to the slowest vehicle speed that has the highest displacement values. Pitch displacement values are rather higher than roll's yet these values are so small, the highest value is rather smaller than 1^o, that they could be considered negligible. For the first road irregularity profile, the speed graphs of the full vehicle model are shown in Figure 5. Like displacement graphs, it is observed that the velocity values decrease as vehicle speed increases. The changes in car body speed are greater compared to the ones at the passenger seat. Pitch and roll movement velocities and displacement values are low.

Acceleration graphs of the full vehicle model are shown in Figure 6. Like the displacement and velocity graphs, acceleration values decrease when vehicle speed increases. While passenger seat acceleration at the lowest vehicle speed is in the "extremely uncomfortable" region, as the vehicle speed increases, it moves towards the "uncomfortable" region. As for the car body acceleration, both vertical and pitch movement accelerations are in the "extremely uncomfortable region", according to ISO 2631-1 [31, 33]. As vehicle speed increases, peak values locations exist more at the right side for all accelerations as in the displacement figures. This situation shows that the spring stiffness and the damping coefficient of the passenger and the vehicle body are not suitable and need to be reconsidered. When the passenger acceleration is taken into consideration, it is observed that the values obtained are not suitable for driving comfort. Roll movement accelerations are not considered high when compared with the pitch values. The force graphs of the full vehicle model are shown in Figure 7. Acting forces upon the passenger seat are not high, and like displacement, velocity, and acceleration graphs, when the speed of the vehicle increases, these values decrease and peak point locations move towards to the right side. When the forces acting on the vehicle body are examined, it is observed that the forces in the roll movement direction are not too high. But vertical and pitch direction forces have high-level values, and thus, they could be harmful to the car body equipment especially considering the bearing location.

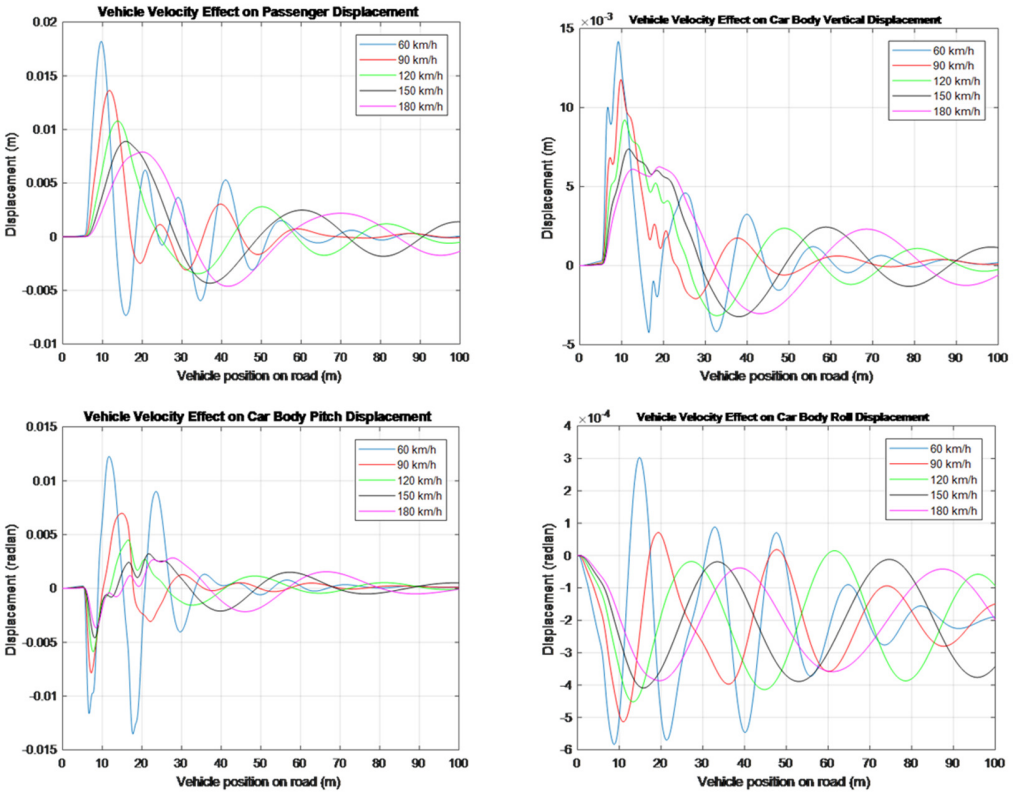

Fig. 4. For the first road irregularity profile: passenger seat vertical displacement and car body vertical, pitch, and roll movement displacements

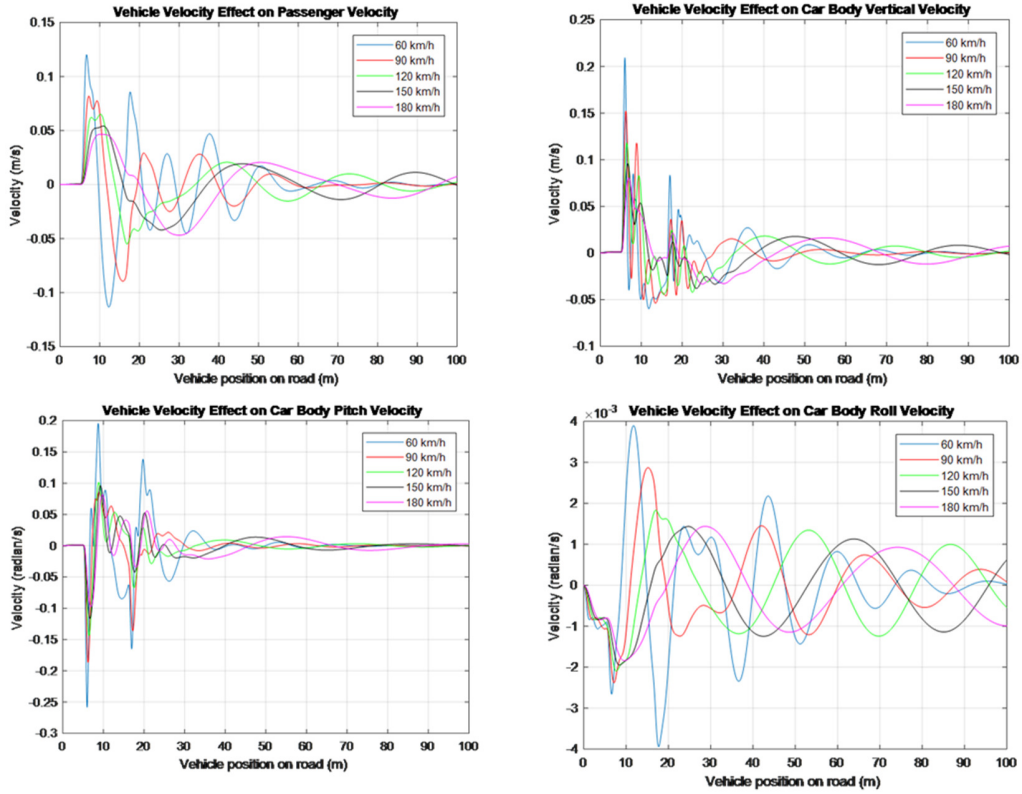

Fig. 5. For the first road irregularity profile: passenger seat vertical velocity, car body vertical, pitch, and roll movement velocities

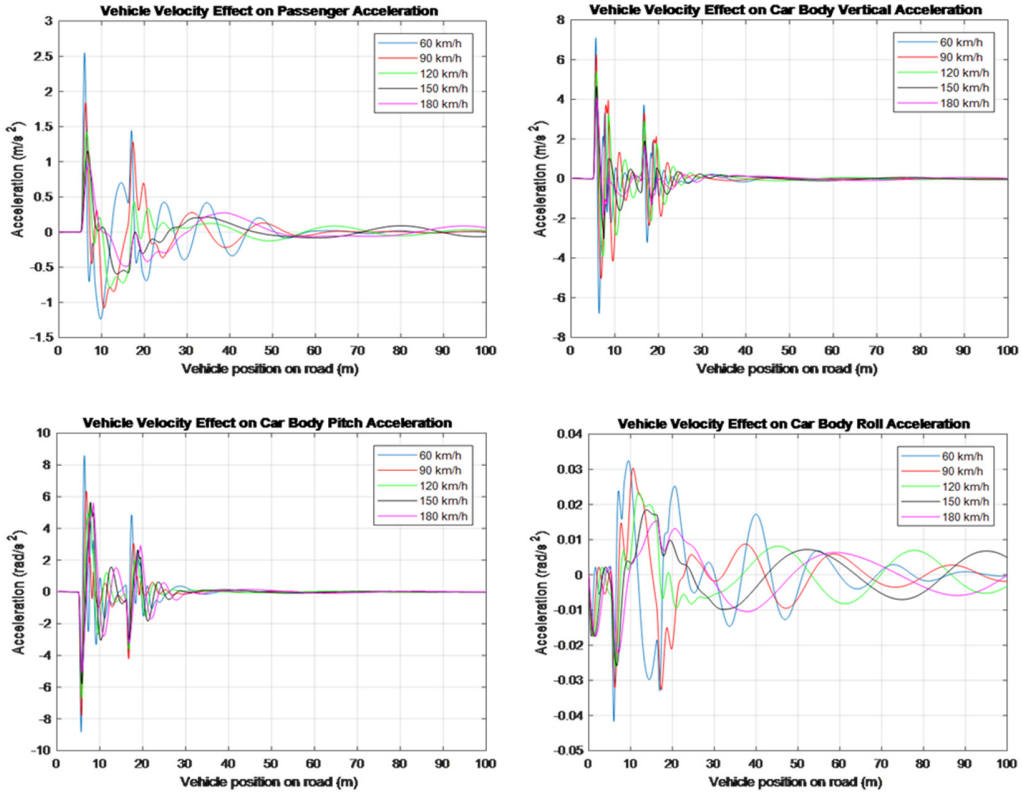

Fig. 6. For the first road irregularity profile: passenger seat vertical acceleration, car body vertical, pitch, and roll movement accelerations

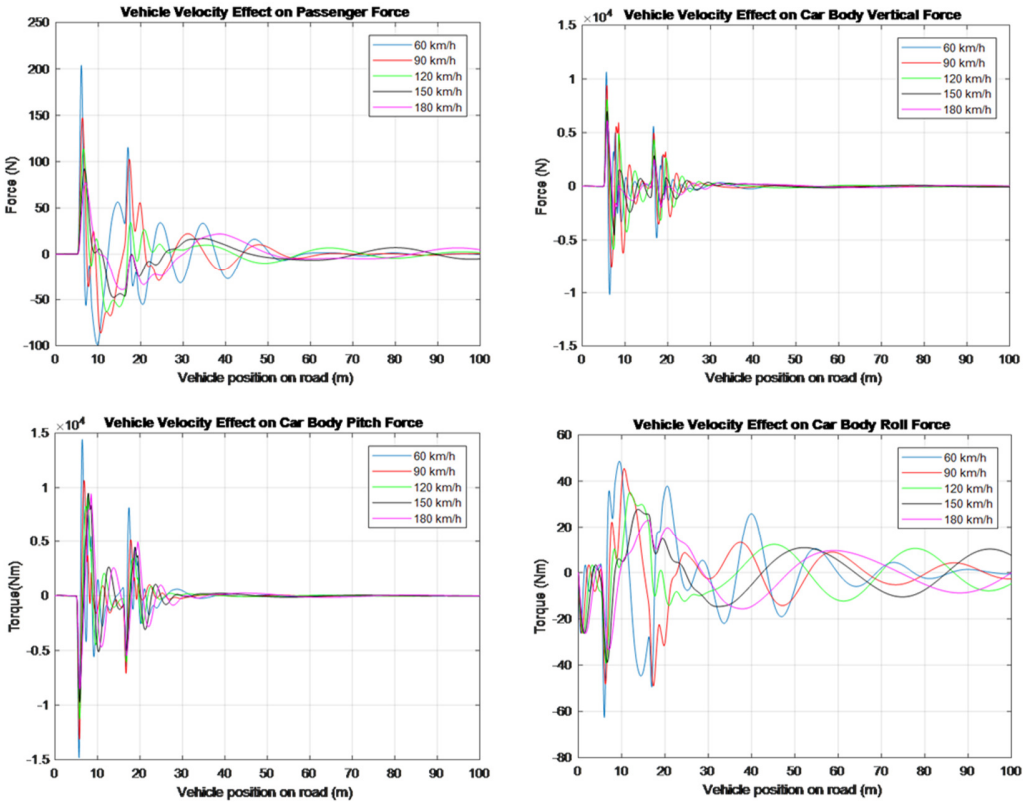

Fig. 7. For the first road irregularity profile: passenger seat vertical force, car body vertical, pitch, and roll movement forces

B. Results of the Second Road Irregularity

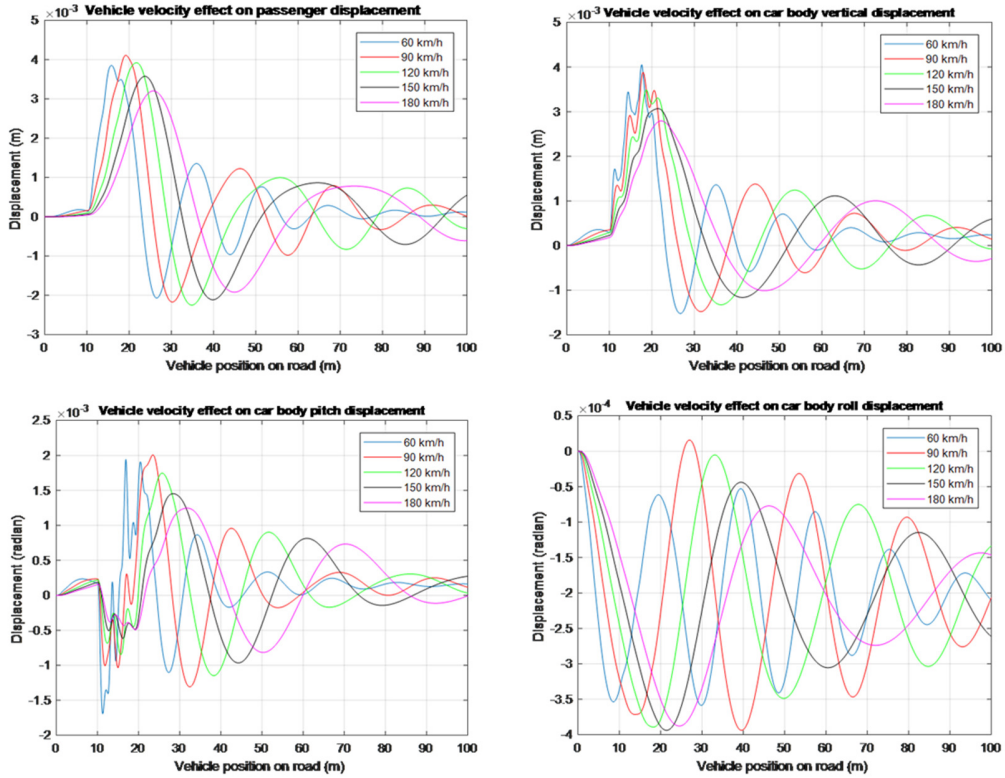

Fig. 8. For the second road irregularity profile: passenger seat vertical displacement, car body vertical, pitch, and roll movement displacements

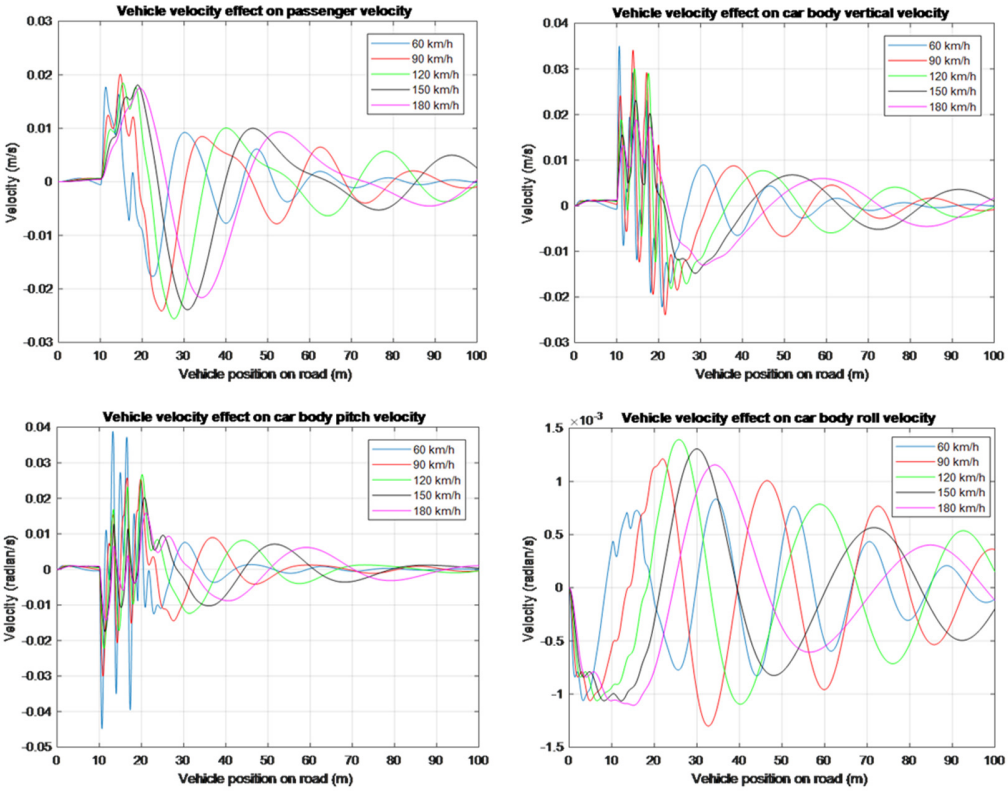

Fig. 9. For the second road irregularity profile: passenger seat vertical velocity, car body vertical, pitch, and roll movement velocities

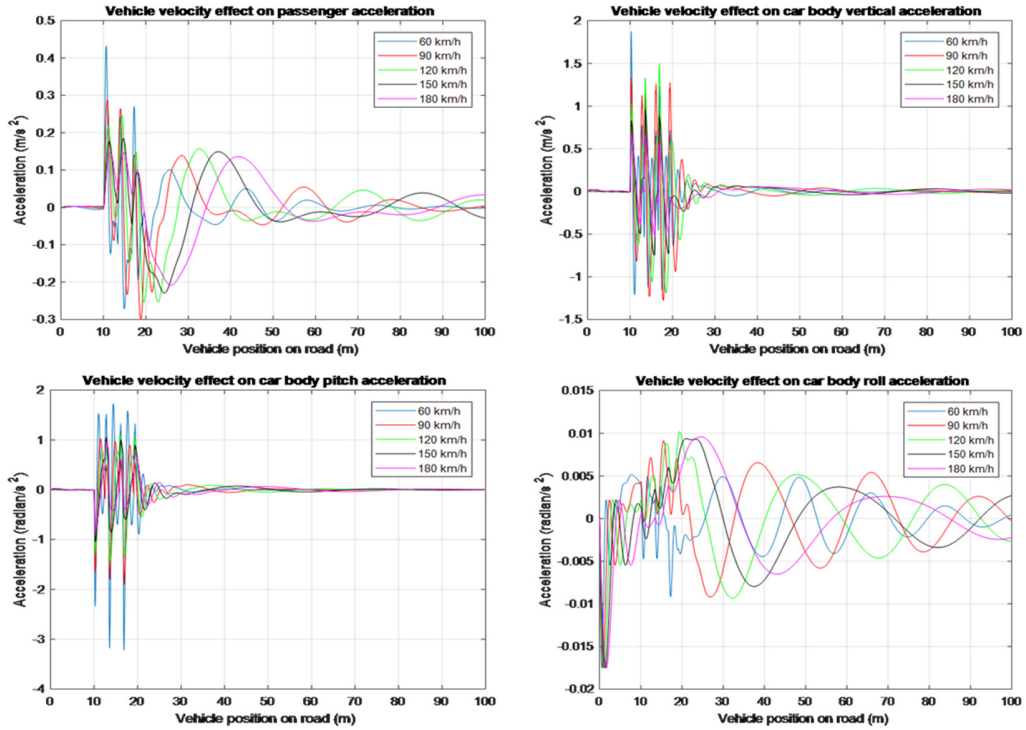

Fig. 10. For the second road irregularity profile: passenger seat vertical acceleration, car body vertical, pitch, and roll movement accelerations

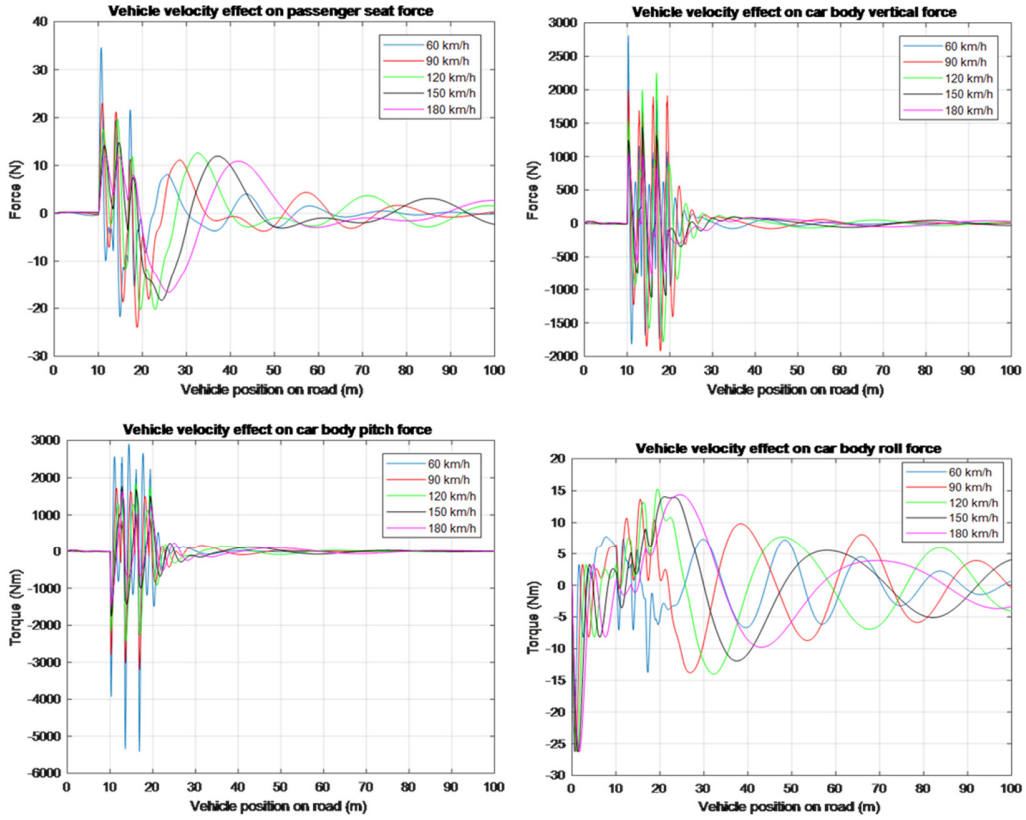

Fig. 11. For the second road irregularity profile: passenger seat vertical force, car body vertical, pitch, and roll movement forces

The second road irregularity profile is given in Figure 3. Under this road irregularity, change of passenger seat vertical displacement and car body vertical, pitch, and roll displacements are shown in Figure 8, for five different vehicle velocities. It is observed that there is a decrease in the magnitude of displacement values that occur as vehicle speed increases. The peaks of the displacement values occur more on the right side, as in the first road graphs. In these graphs, this situation differs slightly for the first speed only and this is probably due to the fact that the bumps are closer to each other. The velocity graphs are shown in Figure 9. We can see that speed amplitude increases as vehicle speed increases from 60 to 120km/h, while speed amplitude decreases as vehicle speed increases from 120 to 180km/h. The acceleration graphs are shown in Figure 10. While passenger seat acceleration at the lowest vehicle speed is in the "little uncomfortable" region, as the vehicle speed increases, it moves towards the "not uncomfortable" region, according to ISO 2631-1. When the passenger comfort is taken into consideration, it could be said that the obtained values provide driving comfort. Also, compared with the first road profile, it is observed that while the amplitudes are reduced by half, in acceleration values significant decreases occur. According to the ISO 2631-1 standard, the acceleration values are changing from the "extremely uncomfortable" region to the "little uncomfortable" region. Both the vertical and the pitch accelerations of the car body are in the "extremely uncomfortable" region. This shows that the acceleration values on the vehicle body are at undesirable levels. Roll movement accelerations are not high when compared with pitch values. According to Figure 11, vehicle roll movement force and passenger vertical force have low amplitude levels. This shows that the equipment of the passenger seat is under the suitable condition. Similarly, bearing equipment of the car body is not under high-level force considering roll movement. As for the vertical and the pitch movement forces, they don't have low but high force values. The car body equipment should be designed considering these dynamic acting forces.

VI. CONCLUSIONS

The main contribution of this study is the analysis of the forces applied to the vehicle body and the driver's seat. For dynamical analysis, the Newmark average acceleration method was used, which is not common in the literature. In this paper, the full vehicle model was considered and the dynamical behaviors of the vertical and rotational movements have been analyzed for the driver's seat and the car body. Two different road irregularity models were created and analysis was run with Newmark average acceleration method. For the first road irregularity, accelerations are in the "extremely uncomfortable" region except for the roll movement accelerations. When the second road profile was examined, as the amplitude of the road profile disturbance was halved, it is seen that the acceleration values pass to the "little uncomfortable" and "not uncomfortable" regions according to the ISO 2631-1 standard. For the first road profile, the vertical force and the pitch movement force of the car body have high values, and thus the equipment of the vehicle should be designed considering these forces. Similar with the acceleration values, under the second road profile irregularity, road disturbance amplitude was halved and the vertical and the pitch forces values of the car body were significantly decreased. The forces of the seat and the roll movement of the car body were not in a high-level for both road profiles. On the other hand, as the vehicle speed increased, it was observed that there was an increase in the period of movement of both the vehicle and the seat.

REFERENCES

[1] R. N. Yerrawar, R. R. Arakerimath, "Parametric analysis of magnetorheological strut for semiactive suspension system using Taguchi method", Engineering, Technology & Applied Science Research, Vol. 8, No. 4, pp. 4561-4565, 2018

[2] P. Sharma, N. Saluja, D. Saini, P. Saini, "Analysis of automotive passive suspension system with Matlab program generation", International Journal of Advancements in Technology, Vol. 4, No. 2, pp. 115-119, 2013

[3] Y. Shen, L. Chen, X. Yang, D. Shi, J. Yang, "Improved design of dynamic vibration absorber by using the inerter and its application in vehicle suspension", Journal of Sound and Vibration, Vol. 361, pp. 148-158, 2016

[4] E. A. Sanchez, "A quarter-car suspension system: Car body mass estimator and sliding mode control", Procedia Technology, Vol. 7, pp. 208-214, 2013

[5] A. J. Qazi, A. Khan, M. T. Khan, S. Noor, "A parametric study on performance of semi-active suspension system with variable damping coefficient limit", AASRI Procedia, Vol. 4, pp. 154-159, 2013

[6] F. Pehlivan, C. Mizrak, I. Esen, "Modeling and validation of 2-DOF rail vehicle model based on electro–mechanical analogy theory using theoretical and experimental methods", Engineering, Technology & Applied Science Research, Vol. 8, No. 6, pp. 3603-3608, 2018

[7] A. Tandel, A. R. Deshpande, S. P. Deshmukh, K. R. Jagtap, "Modeling, analysis and PID controller implementation on double wishbone suspension using simMechanics and simulink", Procedia Engineering, Vol. 97, pp. 1274-1281, 2014

[8] B. Gururaj, K. S. Gowri, "Performance optimization of an eCAR by parametric analysis", Engineering, Technology & Applied Science Research, Vol. 9, No. 6, pp. 4968-4973, 2019

[9] T. Yoshimura, A. Kume, M. Kurimoto, J. Hino, "Construction of an active suspension system of a quarter car model using the concept of sliding mode control", Journal of Sound and Vibration, Vol. 239, No. 2, pp. 187-199, 2001

[10] K. Rejaswari, S. Lavanya, P. Lakshmi, "Grey fuzzy sliding mode controller for vehicle suspension system", CEAI, Vol. 17, No. 3, pp. 12-19, 2015

[11] E. Yildirim, I. Esen, "Using newmark beta method for quarter car analysis", 4th International Conference on Engineering and Natural Science, Kiev, Ukraine, May 2-6, 2018

[12] A. H. Galal, "Car dynamics using quarter model and passive suspension, part VI: Sprung-mass step response", Journal of Computer Engineering, Vol. 17, No. 2, pp 65-74, 2015

[13] X. Ning, C. Zhao, J. Shen, "Dynamic analysis of car suspension using ADAMS/Car for development of a software interface for optimization", Procedia Engineering, Vol. 16, pp. 333-341, 2011

[14] O. Demir, I. Keskin, S. Cetin, "Modeling and control of a nonlinear half-vehicle suspension system: A hybrid fuzzy logic approach", Nonlinear Dynamics, Vol. 67, pp. 2139-2151, 2012

[15] C. J. Huang, J. S. Lin, C. C. Chen, "Road-adaptive algorithm design of half-car active suspension system", Expert Systems with Applications, Vol. 37, No. 6, pp. 4392-4402, 2010

[16] Y. Jin, X. Luo, "Stochastic optimal active control of a half-car nonlinear suspension under random excitation", Nonlinear Dynamics, Vol. 72, pp. 185-195, 2013

[17] H. Hajkarami, H. Samandari, S. Z. Rad, "Analysis of chaotic vibration of a nonlinear seven degress-of-freedom full vehicle model", 3rd International Conference on Integrity, Reliability and Failure, Porto, Portugal, July 20-24, 2009

[18] B. Creed, N. Kahawatte, S. Varnhagen, "Development of a full car vehicle dynamics model for use in the design of an suspension control system", MAE 272-Winter-Paper I, University of California, 2010

[19] A. Shirahatti, P. S. S. Prasad, P. Panzade, M. M. Kulkarni, "Optimal design of passenger car suspension for ride and road holding", Journal of the Brazilian Society of Mechanical Sciences and Engineering, Vol. 30, No. 1, pp. 66-76, 2008

[20] M. Paksoy, R. Guclu, S. Cetin, "Semiactive self-tuning fuzzy logic control of full vehicle model with MR damper", Advances in Mechanical Engineering, Vol. 6, pp. 816-813, 2014

[21] P. Brezas, M. C. Smith, W. Houlth, "A clipped-optimal control algorithm for semi-active vehicle suspensions: Theory and experimental evaluation", Automatica, Vol. 53, pp. 188-194, 2015

[22] M. Q. Nguyen, J. M. Gomes da Silva Jr, O. Seneme, L. Dugard, "A state feedback input constrained control design for a 4-semi-active damper suspension system: A quasi-LPV approach", IFAC-PapersOnLine, Vol. 48, No. 14, pp. 259-264, 2015

[23] A. Unger, F. Schimmack, B. Lohmann, R. Shwarz, "Application of LQ-based semi-active suspension control in a vehicle", Control Engineering Practice, Vol. 21, No. 12, pp. 1841-1850, 2013

[24] L. Dugard, O. Sename, S. Aubouet, B. Talon, "Full vertical car observer design methodology for suspension control applications", Control Engineering Practice, Vol. 20, No. 9, pp. 832-845, 2012

[25] A. H. Galal, N. A. A. Mohammed, "Frequency response of 10 degrees of freedom full-car model for ride comfort", International Journal of Scientific Research Engineering & Technology, Vol. 4, No. 1, pp. 43-49, 2015

[26] D. B. Hassen, M. Miladi, M. S. Abbes, S. C. Baslamisli, F. Chaari, M. Hadder, "Road profile estimation using the dynamic responses of the full vehicle model", Applied Acoustics, Vol. 147, pp. 87-99, 2019

[27] G. G. Fossati, L. F. F. Miguel, W. J. P. Casas, "Multi-objective optimization of the suspension system parameters of a full vehicle model", Optimization and Engineering, Vol. 20, pp. 151-177, 2019

[28] H. Jing, R. Wang, C. Li, J. Bao, "Robust finite-frequency H∞ control of full-car active suspension", Journal of Sound and Vibration, Vol. 441, pp. 221-239, 2019

[29] A. Kruczek, A. Stribrsky, "A full-car model for active suspension-some practical aspects", IEEE International Conference on Mechatronics, Istanbul, Turkey, June 5-5, 2004

[30] A. F. Jahromi, A. Zabihollah, "Linear quadratic regulator and fuzzy controller application in full-car model of suspension system with magnetorheological shock absorber", IEEE/ASME International Conference on Mechatronics and Embedded Systems and Applications, Qingdao, China, July 15-17, 2010

[31] M. A. Koc, I. Esen, "Modelling and analysis of vehicle-structure-road coupled interaction considering structural flexibility, vehicle parameters and road roughness", Journal of Mechanical Science and Technology, Vol. 31, No. 5, pp. 2057-2074, 2017

[32] http://pioneer.netserv.chula.ac.th/~cchatpan/2101606/Ch5.pdf

[33] https://www.iso.org/standard/7612.html